Journal of Structural Geology 37 (2012) 65–74

Contents lists available at SciVerse ScienceDirect

Journal of Structural Geology

journal homepage: www.elsevier.com/locate/jsg

The causes of sinuous crustal-scale deformation patterns in hot orogens: Evidence from scaled analogue experiments and the southern Central Andes

Ulrich Riller[a,*], Alexander R. Cruden[b,c], David Boutelier[b], Christoph E. Schrank[d]

[a] School of Geography and Earth Sciences, McMaster University, 1280 Main Street West, Hamilton, Ontario L8S 4K1, Canada
[b] School of Geosciences, Monash University, Melbourne, Victoria 3800, Australia
[c] Department of Geology, University of Toronto, Toronto, Ontario M5S 3B1, Canada
[d] School of Earth and Environment, The University of Western Australia, 35 Stirling Highway, Crawley WA 6009, Australia

ARTICLE INFO

Article history:
Received 6 September 2011
Received in revised form
28 January 2012
Accepted 1 February 2012
Available online 9 February 2012

Keywords:
Analogue modelling
Central Andes
Plateau formation
Transpression
Basin formation

ABSTRACT

The cause of upper-crustal segmentation into rhomb-shaped, shear zone-bound domains associated with contractional sedimentary basins in hot, wide orogens is not well understood. Here we use scaled multilayered analogue experiments to investigate the role of an orogen-parallel crustal-strength gradient on the formation of such structures. We show that the aspect ratio and size of domains, the sinuous character and abundance of transpressional shear zones vary with the integrated mechanical strength of crust. Upper-crustal deformation patterns and the degree of strain localization in the experiments are controlled by the ratio between the brittle and ductile strength in the model crust as well as gradients in tectonic and buoyancy forces. The experimental results match the first-order kinematic and structural characteristics of the southern Central Andes and provide insight on the dynamics of underlying deformation patterns in hot, wide orogens.

1. Introduction

Hot orogens are characterized by high crustal heat flow, pervasive felsic magmatism, large widths and distributed deformation (Collins, 2002; Chardon et al., 2009; Cruden et al., 2006; Beaumont et al., 2010). Hot orogens are well known from Precambrian and Paleoproterozoic terrains, such as the western Superior Province and Trans-Hudson orogens, Canada (Park, 1981; Gapais et al., 2005), the Yilgarn Craton, Australia (Davis and Maidens, 2003), the Dharwar Craton, India (Bouhallier et al., 1993; Chardon et al., 2002) and the Svecofennides in Finland (Ehlers et al., 1993). A prominent structural characteristic of these partially exhumed hot orogens is the presence of anastomosing zones of ductile transpressional deformation (e.g., Ehlers et al., 1993; Chardon et al., 2002, 2009; Gapais et al., 2005). These deformation zones are conjugate and subvertical. The geometry and kinematics of the zones suggest that the crust of these hot orogens underwent bulk inhomogeneous shortening (Choukroune et al., 1987; Gapais et al., 1987) that was compensated mostly by orogen-parallel rather than vertical stretching (Gapais et al., 2005; Chardon et al., 2009). This deformational behaviour is attributed to an overall mechanically weak crust or lithosphere (Cagnard et al., 2006; Chardon et al., 2009) compressed between stronger blocks or vises (Cruden et al., 2006).

In addition to field studies, the structural and kinematic evolution of hot orogens has been examined by means of analogue experiments, in which uniformly stratified model crust was shortened and forced to escape laterally (Cagnard et al., 2006; Cruden et al., 2006). The experiments generated horizontal strain fabrics in the lower crust and subvertical fabrics in the upper crust, corresponding to structures observed in natural prototypes (Ehlers et al., 1993; Hudleston et al., 1988; Chardon et al., 2002; Choukroune et al., 1995). The experiments also reproduced the anastomosing geometry of mid- to upper-crustal transpression zones observed in exhumed hot orogens.

The Central Andes (Fig. 1) are a type example of an actively forming hot orogen. In the southern Central Andes, notably the Puna Plateau and fold-thrust belts to the east and south, transpressive deformation zones generated morphological ranges, which envelop elliptical to rhomb-shaped sedimentary basins (Fig. 1b). As a consequence, deformation zones in these areas form an anastomosing pattern. The mechanical origin of the rhomb-shaped basins and enveloping deformation zones is not well understood. The geometry and kinematics of deformation zones

* Corresponding author.
E-mail address: rilleru@mcmaster.ca (U. Riller).

0191-8141/$ – see front matter © 2012 Elsevier Ltd. All rights reserved.
doi:10.1016/j.jsg.2012.02.002

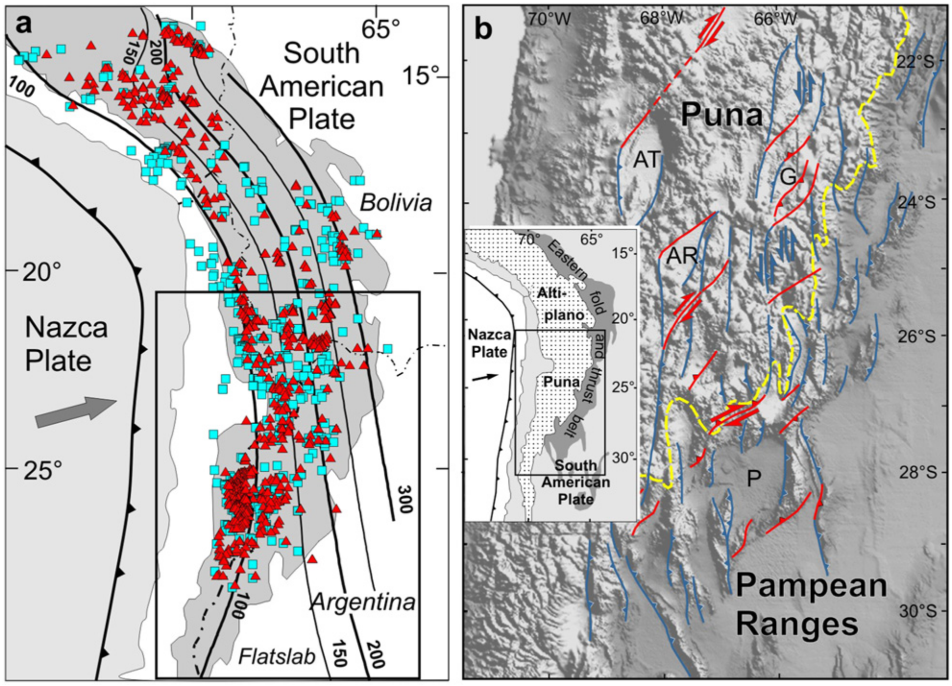

Fig. 1. Major magmatic and structural characteristics of the Central Andes. (a) Location of post-30 Ma magmatic centres (red triangles) and ignimbrites (blue squares) based on a compilation by Trumbull et al. (2006). Grey shading shows elevations above 3000 m. Black lines are slab depth contours in kilometres from Cahill and Isacks (1992). Rectangle denotes area in (b). (b) Morpho-tectonic map of the southern Central Andes showing the rhomb-shaped geometry of major Neogene compressional basins (AT: Salar de Atacama, G: Salinas Grandes, AR: Salar de Arizaro, P: Salar de Pipanaco) and orogen-parallel (blue) and NE-striking (red) fault zones. The yellow dashed line indicates the trace of the eastern margin of the internally drained plateau margin as defined by the 3000 m elevation contour (Gephart, 1994). For kinematics of fault zones see Riller and Oncken (2003). Inset shows the Altiplano-Puna Plateau (hatched) as defined by the 3000 m elevation contour (Gephart, 1994). (For interpretation of the references to colour in this figure legend, the reader is referred to the web version of this article.)

have been attributed to an along-strike gradient in the magnitude of crustal shortening in the southern Central Andes (Riller and Oncken, 2003). This gradient may have induced a strong plan-view simple shear component parallel to the trace of the symmetry plane of the Andean orocline, which trends ENE–WSW (Gephart, 1994). The resulting horizontal sectional strain ellipse contains two directions of maximum, but complementary, shear strains. The shear strain directions agree with dextral shear observed on NE-striking deformation zones and sinistral shear evident on orogen-parallel deformation zones (Fig. 1b). The propagation and coalescence of the deformation zones can account for their anastomosing pattern. Such a gradient is well justified by balanced cross sections for the fold and thrust belt to the east of the Puna Plateau (Kley and Monaldi, 1998). However, the strain gradient may not be large enough or the sole cause of the rhomb-shaped basins in the Puna Plateau and adjacent fold-thrust belts.

Post-30 Ma volcanism (Fig. 1a) has affected much of the Puna Plateau between 20°S and 28°S (Trumbull et al., 2006). In particular, there is a pronounced southward decrease in the east–west extent of magmatic centres and occurrences of ignimbrites that erupted from large 10 Ma to 2 Ma collapse calderas (Fig. 1a). The ignimbrites represent an episode of widespread crustal melting that coincides with enhanced shortening rates in the Central Andes (Oncken et al., 2006). This suggests that the crust was weakened by magmatism and this is supported by the presence of a mid-crustal zone of partial melting that has been imaged geophysically between 19°S and 25°S (Schmitz et al., 1997; Yuan et al., 2000; Oncken et al., 2003). The upper boundary of this zone corresponds approximately to the depth (7–11 km) at which the magmas of large-volume felsic ignimbrites formed (Lindsay et al., 2001; Petrinovic et al., 2005). The southward narrowing of the area containing abundant Neogene magmatic centres suggests that crustal strength should also increase in this direction. The effect of a crustal-strength gradient on the structural evolution of the upper crust has never been examined for the southern Central Andes but can be tested using analogue experiments.

We use multilayer analogue experiments to explore the possible effect of an orogen-parallel crustal-strength gradient on the structural evolution of the southern Central Andes. Specifically, we focus on the morpho-tectonic evolution as well as pattern and kinematics of prominent deformation zones of this region. The modelling results are evaluated in terms of brittle-to-ductile strength (Γ) and buoyancy-to-strength (Ar) ratios. The evolution of deformation patterns is analysed using an optical strain monitoring system and the results are compared to the structure and kinematics of upper-crustal deformation of the Puna Plateau and adjacent fold-thrust belts (Fig. 1b).

2. Tectonic setting of the Puna Plateau

The morpho-tectonic evolution of the Andes is commonly attributed to the geometry of the subducted Nazca Plate and, to a lesser extent, the pre-Andean configuration of the crust (Jordan et al., 1983; Gephart, 1994; Allmendinger et al., 1997). At about 27°S in the southern Central Andes, there is a marked morpho-tectonic transition from distributed deformation within the upper crust in the Puna Plateau and its eastern foreland to localized deformation in the Pampean Ranges, evident from isolated basement uplifts making up the ranges (Fig. 1b). This transition has been ascribed to the change from "steep" (~30°) to flat-slab (~5°–10°) subduction, respectively, of the Nazca Plate (Jordan et al., 1983; Allmendinger et al., 1997). However, the overall width of the orogen is about the same to the north and south of the morpho-tectonic transition and therefore does not correlate with the present geometry of the subducted Nazca Plate.

The direction and velocity of relative plate motion between the Nazca Plate and the South American Plate varied considerably during Mesozoic to Cenozoic times (Pardo-Casas and Molnar, 1987). Changes in the kinematics of major coast-parallel fault zones within the present forearc during the Mesozoic have been attributed to changes in relative plate motion (Scheuber and Andriessen, 1990). The Neogene to Recent plate convergence vector between the Nazca Plate and the South American Plate trends N75°E at the latitude of the southern central Andes (Pardo-Casas and Molnar, 1987; Norabuena et al., 1999). The resulting obliquity between this vector and the plate interface is considered to have influenced the kinematics of deformation in the forearc (Dewey and Lamb, 1992), although Neogene to Recent deformation in this area is dominated by horizontal E–W extension and compression due to processes associated with subduction erosion (Adam and Reuther, 2000; González et al., 2003; Allmendinger and González, 2010). It remains to be determined whether Neogene to Recent relative plate motion influenced the kinematics of deformation east of the forearc.

The Puna Plateau (Fig. 1b) formed by Eocene to Recent east–west crustal shortening (Jordan et al., 1983; Isacks, 1988; Allmendinger et al., 1997). Shortening led to segmentation of the upper crust into rhomb-shaped deformation domains (Riller and Oncken, 2003), which correspond spatially to internally drained, contractional Neogene sedimentary basins (Sobel et al., 2003; Kraemer et al., 1999). Basin size increases from north to south, whereas the number and aspect ratio of the basins decrease (Fig. 1b). Basins in the Puna Plateau are confined by pronounced morphological ranges, which formed by oblique reverse faulting and kilometre-scale folding of Paleozoic basement and Cenozoic cover rocks (Allmendinger et al., 1997; Coutand et al., 2001). The kinematics of these deformation zones is constrained by fault-fold relationships, fault-slip analysis, paleomagnetic analysis and earthquake focal mechanisms (see compilation in Riller and Oncken, 2003). Bulk shortening of the upper crust is accomplished by an anastomosing network of mostly sinistral, orogen-parallel and dextral, NE–SW striking zones of transpressive deformation that are linked kinematically (Coutand et al., 2001; Urreiztieta et al., 1996). The kinematics of deformation associated with basin formation has been attributed to the absolute motion of the South American Plate (Marrett and Strecker, 2000) or an along-strike gradient in the amount of crustal shortening (Riller and Oncken, 2003).

3. Experimental set-up

A rectangular Plexiglas tank was filled with four layers of viscous and granular analogue materials (Fig. 2a, b). The mechanical layering of the model consisted of (1) corn syrup at the base, providing isostatic support to the deforming crust, (2) polydimethysiloxane (PDMS), representing the weak, viscous lower crust, (3) a mixture of PDMS, plasticine and various granular fillers, representing the mechanically stronger but viscous middle crust and (4) granular materials simulating the brittle upper crust (Fig. 2c). A moving piston shortened the model crust at a constant rate while the corn syrup escaped freely below the piston. Hence, we modelled only deformation in the crust. The experiments were monitored with a two-dimensional Particle Imaging Velocimetry (PIV) system to compute high-resolution 2D displacement fields of the model surface (Adam et al., 2005). Dark particles on top of the granular layer served as passive markers for PIV. After shortening, the model upper crust was removed in order to examine the morphology of the model upper-middle crust interface and cross sections were made to observe the structure of the middle and lower crust.

Reference experiments with constant layer thicknesses (Fig. 2a) were conducted to determine the thicknesses of viscous layers that produce fold geometries, which scale approximately to those of the Andes. In the reference experiments (Fig. 2a), with a 6 mm thick mid-crustal viscous layer, fold wavelengths range from 3.4 to 4 cm (Fig. 3). These scale to wavelengths of 54–64 km in nature and match the width of mid-size basins in the central Andes. The reference experiments are characterized by cylindrical folds with hinge lines that trend perpendicular to the imposed shortening direction and span nearly the entire model width (Fig. 3)

The effect of an orogen-parallel strength gradient on deforming crust (Figs. 4, 5) was explored by running an experiment in which the viscous middle and granular upper-crustal layers were characterized by complementary thickness variations parallel to the piston (Fig. 2b). Specifically, the thickness of the viscous layer was 10 mm at one lateral margin and decreased linearly to 2 mm at the opposite margin. The viscous layer and confining PDMS layers were covered by granular upper crust with a thickness of 10 mm above the thin viscous layer margin, grading to 2 mm above the thick

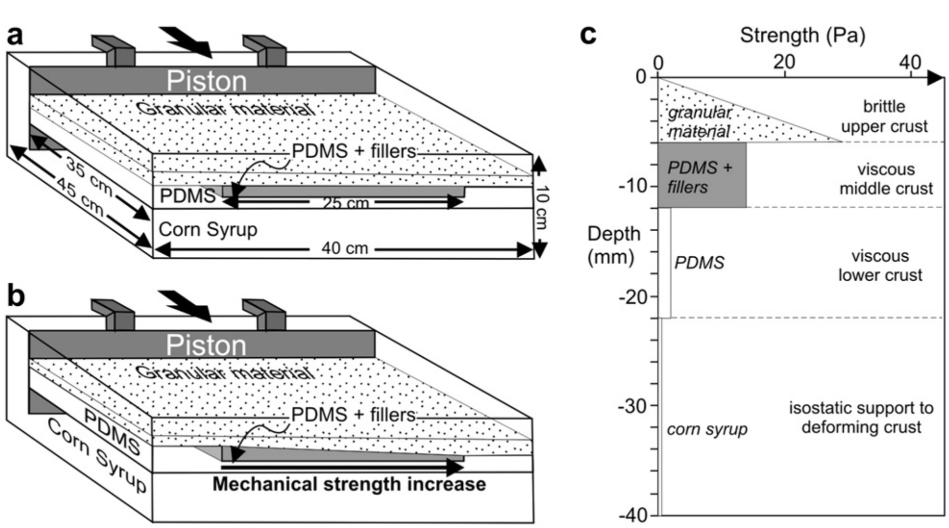

Fig. 2. General set-up of the scaled analogue experiments. (a) Experimental set-up of the control experiments. (b) Experimental set-up of the strength-gradient experiment. (c) Mechanical stratigraphy of analogue materials and equivalent lithological layers.

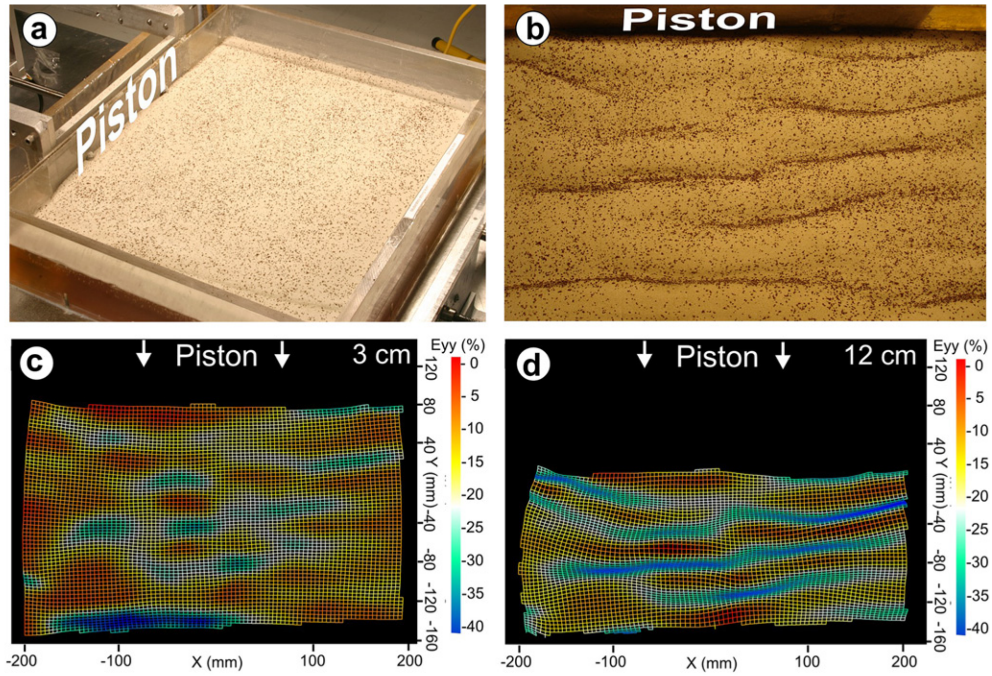

Fig. 3. Photographs and results of Particle Imaging Velocimetry (PIV) of the control experiment with 6 mm thick mid-crustal viscous layer. Cumulative horizontal strain within model deformation zones is indicated by distortion of the Lagrangian mesh computed from the PIV-derived displacement field at the model surface. Colour bars indicate shortening parallel to piston motion. (a) Photograph showing granular upper-crustal layer covered by dark particles (coffee grounds) prior to onset of shortening. (b) Configuration of the upper crust at the end of the experiment. Deformation of granular material is seen by the concentration of dark particles in linear topographic zones, notably uniformly spaced synclines. (c) Cumulative horizontal strain after 3 cm of shortening. (d) Cumulative horizontal strain after 12 cm of shortening.

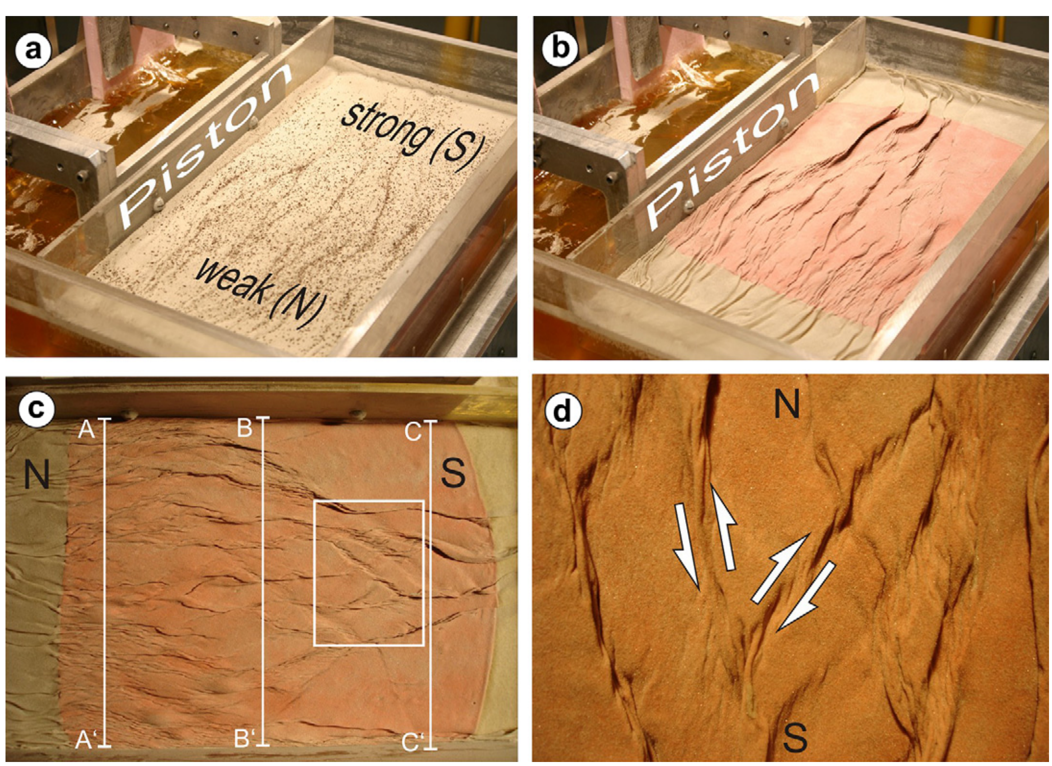

Fig. 4. Photographs showing the final configuration of the granular and viscous layers of the strength-gradient experiment. Letters N and S refer to North and South, respectively, in terms of the Andean reference frame. (a) Geometry of deformation zones in the granular layer highlighted by the concentration of dark particles. (b, c) Geometry of deformation zones in the viscous layer. Rectangle in (c) shows area in (d). Lines A–A′, B–B′ and C–C′ indicate the traces of profiles in Fig. 5. (d) Close-up of (c). Arrows indicate horizontal sense of shear based on the geometry of higher-order folds.

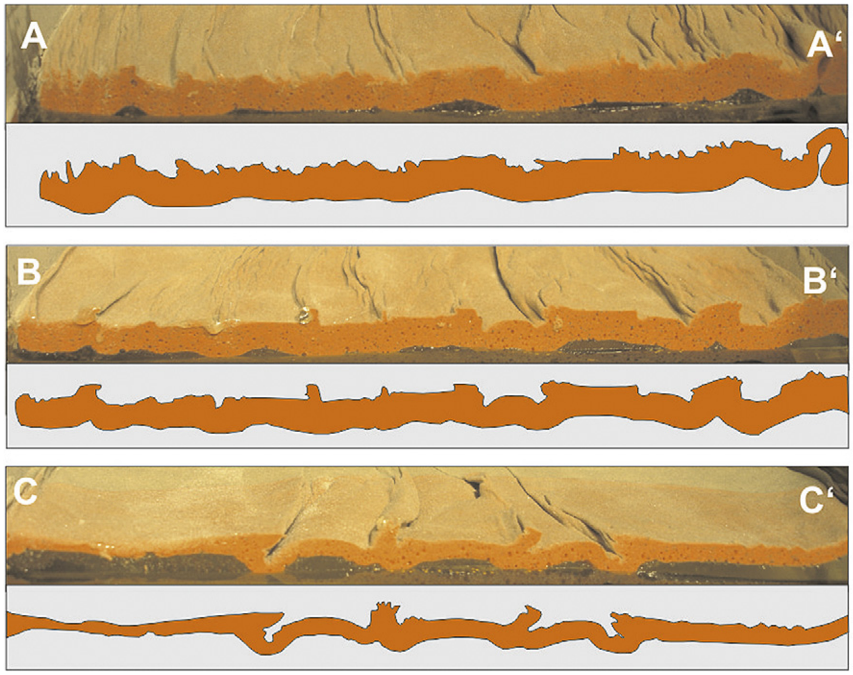

Fig. 5. Photographs and respective line drawings showing the geometry of the middle crustal layer in cross section at selected locations. See Fig. 4c for location of profiles.

layer margin (Fig. 2b). This corresponds, respectively, to an overall strong to weak crustal-strength gradient.

4. Scaling of experimental model parameters and materials

The principal constraints for the design of the laboratory experiments are the physical properties and the length scale of the crust. For practical purposes, a length scale is defined based on a model crustal thickness, $l_m = 2.2$ cm, which for a natural continental crustal thickness $l_p = 36$ km gives a length scale ratio $L = l_m/l_p = 6.1 \times 10^{-7}$ (where the subscripts m and p refer to laboratory and natural prototype, respectively). This length scale allows model orogens equivalent in dimensions to the Central Andes to be generated in a 40 × 45 cm Plexiglas tank (Fig. 2a, b).

Polydimethylsiloxane (PDMS) was used to model the lower crust (Weijermars, 1986; Cruden et al., 2006). It has a density of $\rho_m = 970$ kg/m^3, which for a natural crustal density of $\rho_p = 2800$ kg/m^3, sets a density scale ratio of $P = \rho_m/\rho_p = 0.34$. In the experiments, the gravity scale ratio is $G = g_m/g_p = 1.0$.

At low strain rates, PDMS and PDMS filled with granular materials have a power-law rheology defined by the flow law:

$$\tau^n = \mu\dot{\varepsilon} \quad (1)$$

where τ is shear stress, $\dot{\varepsilon}$ is shear strain rate, μ is a material constant and n is the power-law exponent. The stress exponent of our PDMS is $n = 1.013$ and therefore nearly Newtonian at shear strain rates between 10^{-6} and 10^{-1} s^{-1} (Boutelier et al., 2008). Therefore, PDMS is considered to be a Newtonian fluid with an effective viscosity $\eta_{eff} = \sigma/\dot{\varepsilon}$ of 2.44×10^4 Pa s. Assuming an effective viscosity of $[\eta_{eff}]_p = 10^{21}$ Pa s for the lower crust, a viscosity scale ratio $M = [\eta_{eff}]_m/[\eta_{eff}]_p = 2.5 \times 10^{-17}$ is defined. The time scale ratio for the experiments is then given by $T = M/[PLG] = t_m/t_p = 1.22 \times 10^{-10}$. Therefore 1 h in the experiment corresponds to approximately 1 Ma in nature. The velocity scaling ratio is then given by $V = L/T = U_m/U_p = 4.73 \times 10^3$. The models were shortened at a constant rate of $U_m = 5.6$ mm/h, which corresponds to a natural shortening rate of $U_p = 10$ mm/a. The experiments were stopped after 24 h, corresponding to 22 Ma. The total bulk shortening achieved at the end of the experiments was 38%.

The viscosity of the model middle crustal layer was chosen such that it satisfies the similarity criteria and deforms by buckling rather than uniform thickening during layer shortening. We conducted a series of three-layer buckling experiments (Figs. 2a, 3) in which the composition and strength of the model middle crustal layer was varied systematically while the upper and lower model crust and mantle materials remained unchanged. Buckling of the model middle crust occurred using the following weight percentage mixture: 48% PDMS ($\eta_{eff} = 2.44 \times 10^4$ Pa s) + 29% Harbutt's plasticine (red) + 10% low viscosity PDMS ($\eta_{eff} = 57$ Pa s) + 7% ceramic microspheres + 6% iron filings. This material was used for the viscous middle crust in all experiments and is also slightly non-Newtonian. Over several orders of magnitude of imposed stress, the rheological model determined with a controlled-stress rheometer over an appropriate range of stresses and strain rates is a power law with $n = 1.25$ and $\mu = 3.8 \times 10^5$ Pa^n s. At the typical experimental strain rate (7×10^{-5} s^{-1}) the effective viscosity of this material is 2.0×10^5 Pa s. The model material employed for the strong viscous middle crust has the same density as the viscous lower crust. To minimize gravitational spreading and avoid no-slip boundary effects, the mid-crustal layer was laterally confined by layers of PDMS.

Brittle upper crust was simulated in the experiments with a layer of non-cohesive granular material (cohesion < 30 Pa, stable friction angle < 36°), which is a suitable Mohr–Coulomb analogue (Davy and Cobbold, 1991; Schellart, 2000; Lohrmann et al., 2003). The scaled thickness of the granular layer varied from 2 to 10 mm in different models corresponding to thicknesses of 3.4–16.6 km in nature, respectively. To achieve the desired upper-crustal density (900 kg/m^3), Flexolite glass beads and 3M Z-light ceramic microspheres with bulk densities of 1570 and 440 kg/m^3, respectively, were mixed in the ratio 2.38:1.

The model crust in all experiments was underlain by an 18 mm thick layer of Newtonian corn syrup with a density of 1400 kg/m^3 and a viscosity of 160 Pa s. This is based on the assumption that deformation in the crust is decoupled from that in the lithospheric mantle, whereby the corn syrup layer represents the decoupling horizon and also provides isostatic support.

5. Particle imaging velocimetry

The experiments were observed with a 2D particle imaging velocimetry system (PIV) manufactured by LaVision GmbH (Germany). 2D PIV permits the computation of horizontal surface displacement fields by cross-correlation of sequential images (Adam et al., 2005). One monochrome CCD camera with a sensor of size 1600×1200 pixels was mounted above the model surface at a height of 86 cm. Image resolution was 4.01 pixel/mm. Displacement accuracy was $\pm 97\ \mu m$ and the temporal resolution was 3.3×10^{-2} s. The image recording frequency of 1/600 Hz corresponds to 1 mm piston displacement between successive images. This amounts to a time interval of 10 min between images, which is sufficient to monitor the slow rate of model deformation. For the displacement field calculation, we used square search windows of 16 pixel^2 with 25% overlap. This resulted in a displacement vector spacing of 3 mm and a strain error of $\pm 4.65\%$. Shortening parallel to the piston movement amounts mostly to dip–slip displacement components in model transpression zones and is visualized using the cumulative contractional strain calculated from the Lagrangian cumulative displacement as:

$$E_{yy} = \frac{dD_Y}{dy} \tag{2}$$

where dD_Y is the difference in the y-component of the cumulative displacement of two vectors over the distance dy (y denotes the Cartesian axis parallel to piston motion; dy here equals the displacement vector spacing of 3 mm, (Figs. 3c, d, 6a, c). Rotational deformation around the vertical axis in model transpression zones is visualised using the cumulative vorticity, here defined as the

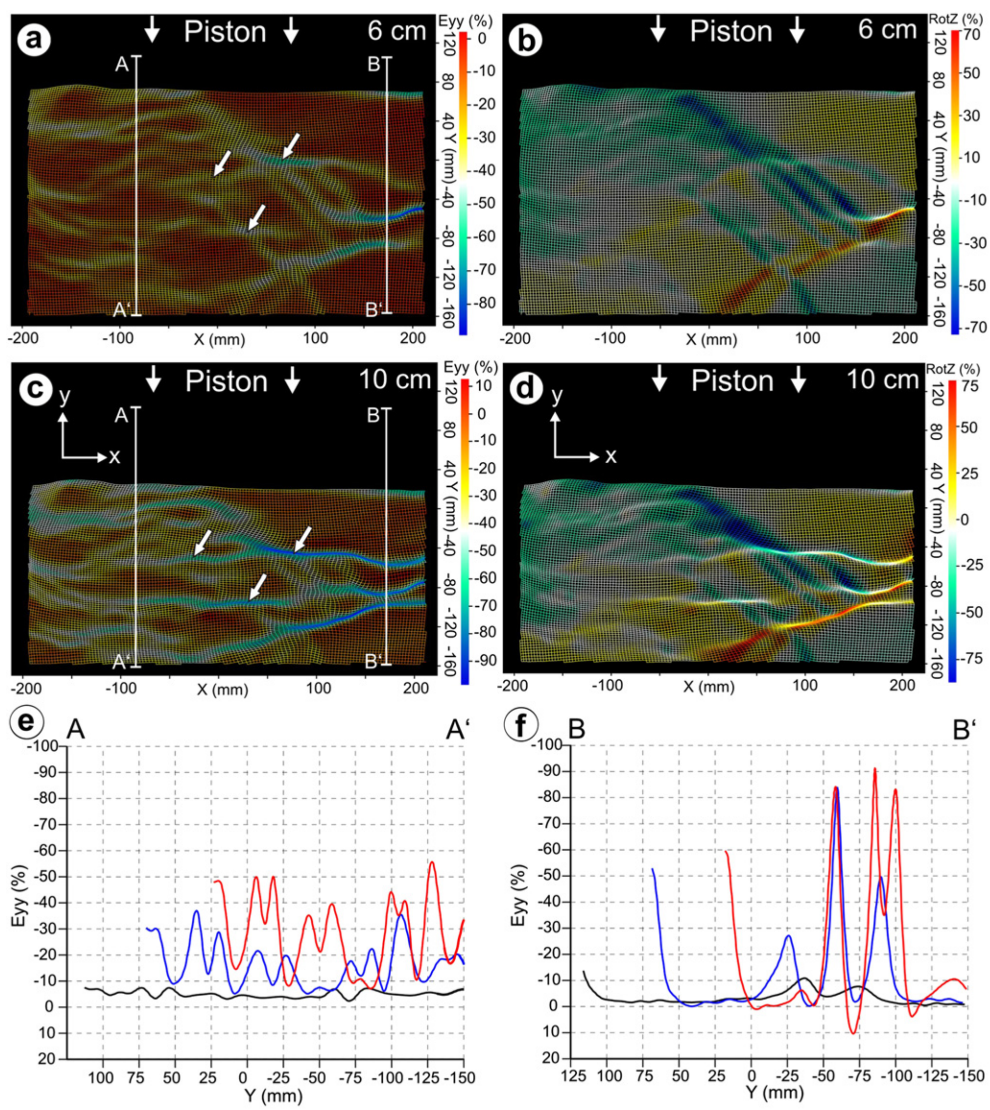

Fig. 6. Particle Imaging Velocimetry (PIV) results of the strength-gradient experiment. (a, c) Cumulative horizontal strain Eyy after 6 cm and 10 cm of shortening. White arrows point to transverse deformation zones that displace, and propagate away from, oblique deformation zones. Profiles A–A′ and B–B′ indicate locations of strain profiles displayed in (e) and (f), respectively. (b, d) Cumulative vorticity (*RotZ*) after 6 cm and 10 cm of shortening. Horizontal strain and sense of shear within model deformation zones is indicated by distortion of the Lagrangian mesh computed from the PIV-derived displacement field of the model surface. Colour bars indicate magnitude of shortening (negative) and extension (positive) parallel to piston motion (a, c) and magnitude of vorticity (positive = sinistral, negative = dextral) (b, d). (e, f) Selected profiles showing horizontal strain Eyy accumulated after 2 cm (black line), 6 cm (blue line) and 10 cm (red line). (For interpretation of the references to colour in this figure legend, the reader is referred to the web version of this article.)

difference of the cumulative shear strains parallel (x) and normal to the piston (y):

$$RotZ = \frac{dD_Y}{dx} - \frac{dD_x}{dy} \quad (3)$$

6. Brittle–ductile ratio and Argand number

In three-layer analogue experiments, the brittle–ductile ratio, Γ (Schueller and Davy, 2008) can be defined as

$$\Gamma = \frac{\rho g h^2}{2U}\left(\frac{1}{\eta_1}+\frac{1}{\eta_2}\right) \quad (4)$$

where ρ and h are the density and thickness of the brittle layer, and η_1 and η_2 are the effective viscosities of the upper and lower ductile layers, respectively. In the analogue shortening experiments reported by Schueller and Davy (2008), localization instabilities were only observed to develop when $\Gamma > 0.5$. Values of Γ in our experiments are reported in Table 1.

The influence of buoyancy forces on lithospheric deformation in natural and analogue orogens can be described using the Argand number (England and McKenzie, 1982),

$$Ar = \frac{F_g}{F_s} \quad (5)$$

where F_g is the vertically integrated buoyancy force that counteracts the build up of lithospheric thickness, and F_s is the vertically integrated strength of the lithosphere acting to resist orogenic collapse. Following England and McKenzie (1982) the buoyancy force acting within the model crust is

$$F_g = \frac{\rho_C g h_C^2}{2}\left(1-\frac{\rho_C}{\rho_M}\right) \quad (6)$$

where h_C and ρ_C are the thickness and density of the model crust and ρ_M is the density of the underlying model mantle. The integrated strength of the model crust is given by

$$F_s = \frac{\rho g h^2}{2} + \dot{\varepsilon}(\eta_1 h_1 + \eta_2 h_2) \quad (7)$$

where h_1 and h_2 are the thicknesses of the ductile middle and lower crust, respectively. Values of Ar in our experiments are reported in Table 1.

7. Experimental results

Accumulations of particles in the strength-gradient experiment mark the traces of reverse faults that collectively define an anastomosing pattern (Fig. 4a). The number of deformation zones and the aspect ratio of enclosed, less deformed crustal domains decreases from the mechanically weak end toward the strong end of the model crust (Figs. 4, 5). Conversely, the rhomb-shaped geometry of less deformed domains becomes more pronounced toward the strong end of the model. These structural characteristics are also evident at the top of the viscous middle crust after removing the granular layer (Fig. 4b–d). The geometry of higher-order, en-echelon fold trains in the viscous layer also accentuates the conjugate pattern of transpressional model deformation zones that envelop rhomb-shaped basins (Fig. 4d). Overall, the amplitudes of first-order buckle folds of the viscous layer increase, whereas the number of higher-order folds of the top surface of this layer decreases toward the strong end of the model (Fig. 5).

PIV imaging records the geometric and kinematic evolution of transpressional deformation zones at the model surface. Horizontal shortening parallel to the piston movement is concentrated in deformation zones enveloping less deformed, elliptical to rhomb-shaped domains (Fig. 6a, c). Maps of cumulative horizontal shortening and vorticity indicate zones that formed orthogonal to the shortening direction and conjugate deformation zones that are oblique to the shortening direction (Fig. 6a–d). Almost all deformation zones formed during initial shortening and, collectively, accumulated the total deformation; overall, the number of deformation zones does not seem to increase during shortening (Fig. 6e, f). Deformation is concentrated in a few zones at the right hand side, the mechanically strongest portion of the model, in contrast to accumulation of deformation in an increasing number of zones toward the mechanically weakest part of the model (Fig. 6a, c). With progressive deformation, deformation zones forming transverse to the shortening direction displace, and propagate away from, initially formed conjugate zones (Fig. 6a, c). Transverse deformation zones take up most of the normal shortening, thereby offsetting conjugate transpression zones. Rhomb-shaped domains enclosed by the transpression zones rotate generally less than 20° during progressive deformation, whereby their rigid-body rotation is close to zero (Fig. 6b, d). Likewise, deformation zones do not rotate much in plan view (Fig. 6a, c) and their conjugate character indicates coaxial deformation on the scale of the analogue model (Fig. 5b, d).

Table 1
Brittle–ductile ratio (Γ), buoyancy force (F_b), integrated crustal strength (F_s) and Argand numbers (Ar) for experiments.

Experiment	Γ	F_b	F_s	Ar
Control experiment	4.70	1.46	0.16	8.83
Strength-gradient experiment: strong end	13.05	1.48	0.44	3.33
Strength-gradient experiment: weak end	0.52	1.44	0.03	52.19

8. Interpretation of experimental results

Previous analogue modeling studies have demonstrated that in brittle–ductile shortening and extension experiments, the spatial density of faults in the brittle layer is reduced when the deformation rate or ductile layer viscosity is decreased or when the thickness of the brittle layer is increased (Schueller and Davy, 2008; Schueller et al., 2010). This effect can be parameterized using the brittle–ductile strength ratio, Γ (Schueller and Davy, 2008). For $\Gamma < 0.5$ deformation in the upper brittle layer tends to be characterized by abundant, distributed faults and folds striking orthogonal to the shortening direction. For increasing values of $\Gamma > 0.5$ deformation becomes progressively localized within a smaller number of transpressional fault zones that strike obliquely to the shortening direction. Similarly, the tendency of the model crust to collapse gravitationally can be described by the Argand number, Ar, which is the ratio between the buoyancy force and the tectonic force (England and McKenzie, 1982; Cruden et al., 2006).

In our calibration experiment $Ar = 8.8$ and in the strength-gradient experiment Ar varied from 3.3 at the strong end to 52.2 at the weak end in the undeformed state (Table 1). Hence there is significant potential for gravitational collapse that could account for the observed along-strike variation in degree of deformation localization. However, because both experiment types are confined laterally, the amount of orogen-parallel flow within the model ductile crust is restricted relative to the amount of convergence and hence the influence of Ar on brittle-layer deformation patterns was likely minor. Nonetheless, some lateral extrusion of the middle crust toward the strong end of the strength-gradient experiment is observed (Fig. 4c). It is conceivable that mid-crustal flow was channelized toward the strong end as a result of a lateral gradient in the gravitational potential that built up during shortening. Such mid-crustal flow may have resulted in gravitational spreading of crust that contributed to the observed anastomosing fault pattern and enhanced strain localization at the strong end of the model (Figs. 4c, 6f) towards which lateral flow is channelled the most.

In the strength-gradient experiment, Γ varies from 13.1 at the strong end to 0.5 at the weak end (Table 1), which corresponds to the empirically observed transition between localized and distributed deformation in brittle–ductile analogue experiments (Schueller and Davy, 2008). Hence, the change from distributed to localized deformation observed on both the surface of the brittle layer (Fig. 4a) and at the brittle–ductile interface (Fig. 4b, c) is consistent with the interpretation that deformation localization in this experiment was controlled by an increase in brittle–ductile ratio from the weak end to the strong end of the model.

9. Discussion

The geometry and kinematic history of deformation zones inferred from nature and experiment can be used to assess the importance of a crustal-strength gradient with regard to other factors contributing to the formation of sinuous deformation patterns in the southern Central Andes. These factors include mainly (1) changes in absolute plate motion, (2) the Neogene obliquity between the Nazca Plate and the South American Plate, (3) an along-strike gradient in crustal (lithospheric) shortening and (4) orogen-parallel extension. The viability of these factors based on published structural data is discussed first and will be followed by delineating the implications of the strength-gradient experiment for the morpho-tectonic evolution of the southern Central Andes.

Shortening and fault zone activity at the eastern margin of the Puna Plateau occurred apparently in distinct pulses and have been related to changes in absolute motion of the South American Plate (Marrett and Strecker, 2000). However, local shortening in the Puna Plateau, Pampean Ranges and eastern fold-thrust belts, inferred from earthquake focal mechanisms and the inversion of brittle shear faults, vary with affinity to prominent fault zones rather than with time and the fault kinematics agree with paleomagnetic rotations (Riller and Oncken, 2003). Specifically, E–W shortening is associated with NW–SE striking zones of sinistral transtension (Riller et al., 2001; Petrinovic et al., 2006; Acocella et al., 2011). NW–SE shortening is commonly linked with orogen-parallel sinistral reverse faults (Urreiztieta et al., 1996; Gapais et al., 2000; Coutand et al., 2001; Riller and Oncken, 2003) and ENE–WSW shortening has been recorded within NE–SW striking dextral reverse fault zones (Marrett et al., 1994; Urreiztieta et al., 1996; Gapais et al., 2000). The simultaneous activity of directionally variable shortening and the fact that absolute plate motion amounts to translation rather than intracontinental deformation, calls into question absolute plate motion as a cause for deformation in the southern Central Andes.

Orogen-parallel, i.e., N–S striking, reverse faults in the Puna Plateau are characterized by components of sinistral displacement (Fig. 1b). However, dextral shear strains should be evident on these faults if the obliquity of Neogene to Recent plate convergence (N75°E: Norabuena et al., 1999) dominated the deformation in the Puna Plateau and its eastern fold-thrust belts. By contrast, an along-strike gradient in crustal shortening may well account for the sinuous pattern of upper crustal, transpressional deformation zones. Such a gradient can result in dextral and sinistral shear zones that match with the orientation and kinematics of conjugate transpressional deformation zones in the southern Central Andes (Riller and Oncken, 2003). The sinuous pattern and kinematics of transpressional deformation zones is also compatible with a component of Neogene orogen-parallel extension indicated by asymmetric collapse of post-10 Ma collapse calderas in the Puna Plateau (Riller et al., 2001; Ramelow et al., 2006). In summary, plate kinematics does not seem to have influenced greatly the kinematics of prominent deformation zones in the southern Central Andes. An along-strike gradient of crustal shortening and orogen-parallel extension, possibly related to formation of the central Andean orocline (Isacks, 1988), are compatible, however, with the observed sinuous deformation pattern, but may not account for the variation in size and aspect ratio of the basins.

Our experimental study highlights the importance of the physical properties of the crust, notably the effect of a crustal-strength gradient, on the morpho-tectonic evolution of orogenic belts, which hitherto has not been considered for the southern Central Andes or other hot orogens. The first-order structural characteristics of the strength-gradient experiment (Fig. 4) are remarkably similar to those in the southern Central Andes (Fig. 1b). In addition to the kinematics of anastomosing deformation zones, both show a variation in (1) aspect ratio and (2) sizes of morpho-tectonic basins, as well as (3) the sinuous character and (4) abundance of deformation zones in relation to the mechanical strength of crust. Shortening throughout the southern Central Andes is inhomogeneous and accomplished by the localization of transpressional deformation zones that bound rhomb-shaped basins. Similar to the transverse deformation zones in the model, orogen-parallel deformation zones in the Puna Plateau are chiefly characterized by shortening and are kinematically linked with transpressional deformation (Fig. 1b). Finally, the kinematic evolution of model deformation zones agrees with the monophase and kinematically uniform, but conjugate, evolution of natural equivalents in the southern Central Andes. Monophase deformation is at variance with hypotheses invoking multiple deformation regimes, such as changes in plate kinematics, for the morpho-tectonic evolution of the Puna and adjacent fold-thrust belts.

The strength gradient can account also for the sinuous and lobate morphological character of the eastern plateau margin, its eastern foreland and the Pampean Ranges (Fig. 1b). Deformation in the eastern foreland and the Pampean Ranges commenced only in late Neogene times and is ongoing (Jordan et al., 1983; Allmendinger et al., 1997). Isolated sinuous basement uplifts in these areas can therefore be interpreted as incipient deformation as a consequence of the crustal-strength gradient. Most importantly, however, it should be noted that the overall style of deformation does not change at the morpho-tectonic transition of the Puna Plateau to the Pampean Ranges. This suggests that the change in the geometry of the subducted Nazca Plate at this transition does not directly influence deformation of the upper plate. The geometry of the subducted Nazca Plate may, however, influence the mechanical strength of the upper plate as the dip of the descending plate controls the lateral extent of magmatism in the upper plate (Fig. 1a). A shallowly dipping Nazca Plate underneath the Pampean Ranges (Fig. 1a) suppresses magmatism (Jordan et al., 1983) and therefore leads to a mechanically strong upper plate, evident from the Salar de Pipanaco, which is the largest and geometrically most prominent example of a rhomb-shaped basin in the southern Central Andes (Fig. 1b).

The strength-gradient experiment features also some lateral escape of viscous middle crust where it is overlain by thick brittle upper crust (Fig. 4c). The flow profile of the escaping middle crust is consistent with the along-strike gradient in *Ar* and matches the polarity of lower crustal channel flow inferred for the Puna Plateau (i.e., from weak toward strong crust) (Hindle et al., 2005; Quimet and Cook, 2010). Channel flow may cause some orogen-parallel extension of the crust, as is evident for the Puna Plateau (Riller et al., 2001). However, based on our strength-gradient experiment, channel flow may not significantly control the geometry and kinematics of crustal deformation, notably the formation of sinuous deformation patterns. The latter is rather a function of the orogen-parallel gradient in the brittle–ductile strength ratio, Γ. Our experiments do not necessarily rule out oblique plate convergence, along-strike gradients in shortening or orogen-prallel extension as contributing factors for the observed fault kinematics but suggest that a crustal-strength gradient should be considered as a major contributor for the morpho-tectonic evolution of the southern Central Andes and other hot orogens.

10. Conclusions

Analogue experiments indicate that a crustal-strength gradient transverse to the shortening direction causes the development of sinuous transpression zones and elliptical to rhomb-shaped basins. In particular, we conclude that strain localization is controlled by the brittle–ductile strength ratio, Γ, which determines the geometry and size of basins and associated deformation zones. Mid-crustal channel flow in the experiment arises from the along-strike variation in *Ar* and may result in limited orogen-parallel extension of the crust. However, channel flow does not significantly control the geometry and kinematics of crustal deformation in our case. The experimental results match the kinematic and geometric characteristics of upper-crustal deformation as well as the topographic variation in the Puna Plateau remarkably well. The results suggest that the first-order morpho-tectonic characteristics of this hot orogen, notably the presence of elliptical to rhomb-shaped deformation domains and bounding sinuous transpressional deformation zones, can be explained by an along-strike crustal-strength gradient. Subduction zone properties, such as plate boundary kinematics, dip of the subducted slab and absolute plate motion seem to be of little importance in this regard. More refined experiments are required to further identify the possible contributions of e.g., orogen-parallel gradients in crustal shortening, plate convergence obliquity, a curved plate interface (Boutelier and Oncken, 2010) and different modes of lithospheric thickening (Allmendinger et al., 1997), to the morpho-tectonic evolution of the southern Central Andes.

Acknowledgements

Experiments were carried out at the University of Toronto Tectonic Laboratory. This work was funded by German Science Foundation (grant Ri 916/9-1 to U.R.) and Natural Sciences and Engineering Council of Canada grants to A.R.C. and U.R. We thank S. Titus for review of an early version of this manuscript. Reviews by D. Gapais and an anonymous referee greatly improved the clarity of this study.

References

Acocella, V., Gioncada, A., Omarini, R., Riller, U., Mazzuoli, R., Vezzoli, L., 2011. Tectonomagmatic characteristics of the back-arc portion of the Calama–Olacapato–El Toro Fault Zone, Central Andes. Tectonics 30, TC3005. doi:10.1029/2010TC002854.

Adam, J., Reuther, C.-D., 2000. Crustal dynamics and active fault mechanics during subduction erosion. Application of frictional wedge analysis on to the North Chilean Forearc. Tectonophysics 321, 297–325.

Adam, J., Urai, J.L., Wieneke, B., Oncken, O., Pfeiffer, K., Kukowski, N., Lohrmann, J., Hoth, S., van der Zee, W., Schmatz, J., 2005. Shear localisation and strain distribution during tectonic faulting—new insights from granular-flow experiments and high-resolution optical image correlation techniques. Journal of Structural Geology 27, 283–301.

Allmendinger, R.W., González, G., 2010. Invited review paper: Neogene to Quaternary tectonics of the coastal Cordillera, northern Chile. Tectonophysics 495, 93–110.

Allmendinger, R.W., Jordan, T.E., Kay, S.M., Isacks, B.L., 1997. The evolution of the Altiplano-Puna Plateau of the Central Andes. Annual Review of Earth and Planetary Sciences 25, 139–174.

Beaumont, C., Jamieson, R., Nguyen, M., 2010. Models of large, hot orogens containing a collage of reworked and accreted terranes. Canadian Journal of Earth Sciences 47, 485–515.

Bouhallier, H., Choukroune, P., Ballèvre, M., 1993. Diapirism, bulk homogeneous shortening and transcurrent shearing in the Archean Dharwar craton: the Holenarsipur area, southern India. Precambrian Research 63, 43–58.

Boutelier, D.A., Oncken, O., 2010. Role of the plate margin curvature in the plateau buildup: consequences for the central Andes. Journal of Geophysical Research 115. article B04402.

Boutelier, D., Schrank, C., Cruden, A.R., 2008. Power-law viscous materials for analogue experiments: new data on the rheology of highly-filled silicone polymers. Journal of Structural Geology 30, 341–353.

Cagnard, F., Durrieu, N., Gapais, D., Brun, J.-P., Ehlers, C., 2006. Crustal thickening and lateral flow during compression of hot lithospheres, with particular reference to Precambrian times. Terra Nova 18, 72–78.

Cahill, T., Isacks, B.L., 1992. Seismicity and shape of the subducted Nazca Plate. Journal of Geophysical Research 97, 17503–17529.

Chardon, D., Peucat, J.-J., Jayananda, M., Choukroune, P., Fanning, C.M., 2002. Archean granite–greenstone tectonics at Kolar (South India): interplay of diapirism and bulk inhomogeneous contraction during juvenile magmatic accretion. Tectonics 21, 1016. doi:10.1029/2001TC901032.

Chardon, D., Gapais, D., Cagnard, F., 2009. Flow of ultra-hot orogens: a view from the Precambrian, clues for the Phanerozoic. Tectonophysics 477, 105–118.

Choukroune, P., Gapais, D., Merle, O., 1987. Shear criteria and structural symmetry. Journal of Structural Geology 9, 525–530.

Choukroune, P., Bouhallier, H., Arndt, N.T., 1995. Soft lithosphere during periods of Archean crustal growth or crustal reworking. In: Coward, M.P.H., Ries, A. (Eds.), Early Precambrian Processes. Geological Society of London Special Publication, vol. 95, pp. 67–86.

Collins, W.J., 2002. Hot orogens, tectonic switching, and creation of continental crust. Geology 30, 535–538.

Coutand, I., Cobbold, P.R., de Urreiztieta, M., Gautier, P., Chauvin, A., Gapais, D., Rossello, E.A., López-Gamundí, O., 2001. Style and history of Andean deformation, Puna plateau, northwestern Argentina. Tectonics 20, 210–234. doi:10.1029/2000TC900031.

Cruden, A.R., Nasseri, M.H.B., Pysklywec, R., 2006. Surface topography and internal strain variation in wide hot orogens from three-dimensional analogue and two-dimensional numerical vice models. In: Buiter, S.J.H., Schreurs, G. (Eds.), Analogue and Numerical Modelling of Crustal-scale Processes. Geological Society, London, Special Publications, vol. 253, pp. 79–104.

Davis, B.K., Maidens, E., 2003. Archaean orogen-parallel extension: evidence from the northern Eastern Goldfields Province, Yilgarn Craton. Precambrian Research 127, 229–248.

Davy, P., Cobbold, P.R., 1991. Experiments on shortening of a 4-layer model of the continental lithosphere. Tectonophysics 188, 1–25.

Dewey, J.F., Lamb, S.H., 1992. Active tectonics of the Andes. Tectonophysics 205, 79–95.

Ehlers, C., Lindroos, A., Selonen, O., 1993. The late Svecofenian granite–migmatite zone of southern Finland – a belt of transpressive deformation and granite emplacement. Precambrian Research 64, 295–309.

England, P.C., McKenzie, D., 1982. A thin viscous sheet model for continental deformation. Geophysical Journal of the Royal Astronomical Society 70, 295–321.

Gapais, D., Balé, P., Choukroune, P., Cobbold, P., Mahjoub, Y., Marquer, D., 1987. Bulk kinematics from shear zone patterns: some field examples. Journal of Structural Geology 9, 635–646.

Gapais, D., Cobbold, P., Bourgeois, O., Roubya, D., Urreiztieta, M., 2000. Tectonic significance of fault-slip data. Journal of Structural Geology 22, 881–888.

Gapais, D., Potrel, A., Machado, N., Hallot, E., 2005. Kinematics of long-lasting Paleoproterozoic transpression within the Thompson Nickel Belt, Manitoba, Canada. Tectonics 24, TC3002. doi:10.1029/2004TC001700.

Gephart, J., 1994. Topography and subduction geometry in the central Andes: clues to the mechanics of a non-collisional orogen. Journal of Geophysical Research 99, 12,279–12,288.

González, G., Cembrano, J., Carrizo, D., Macci, A., Schneider, H., 2003. The link between forearc tectonics and Pliocene–Quaternary deformation of the Coastal Cordillera, northern Chile. Journal of South American Earth Sciences 16, 321–342.

Hindle, D., Kley, J., Oncken, O., Sobolev, S., 2005. Crustal balance and crustal flux from shortening estimates in the Central Andes. Earth and Planetary Science Letters 230, 113–124.

Hudleston, P.J., Schultz-Ela, D., Southwick, D.L., 1988. Transpression in Archean greenstone belts, northern Minnesota. Canadian Journal of Earth Sciences 25, 1060–1068.

Isacks, B., 1988. Uplift of the central Andean plateau and bending of the Bolivian orocline. Journal of Geophysical Research 93, 3,211–3,231.

Jordan, T.E., Isacks, B.L., Allmendinger, R.W., Brewer, J.O.N.A., Ramos, V.A., Ando, C.J., 1983. Andean tectonics related to geometry of subducted Nazca plate. Geological Society of America Bulletin 94, 341–361.

Kley, J., Monaldi, C.R., 1998. Tectonic shortening and crustal thickness in the Central Andes: how good is the correlation? Geology 26, 723–726.

Kraemer, B., Adelmann, D., Alten, M., Schnurr, W., Erpenstein, K., Kiefer, E., van den Bogaard, P., Görler, K., 1999. Incorporation of the Paleogene foreland into the Neogene Puna plateau: the Salar de Antofalla area, NW Argentina. Journal of South American Earth Sciences 12, 157–182.

Lindsay, J.M., Schmitt, A.K., Trumbull, R.B., De Silva, S.L., Siebel, W., Emmermann, R., 2001. Magmatic evolution of the La Pacana Caldera system, Central Andes, Chile: compositionally variation of two cogenetic large-volume felsic ignimbrites. Journal of Petrology 42, 459–486.

Lohrmann, J., Kukowski, N., Adam, J., Oncken, O., 2003. The impact of analogue material properties on the geometry, kinematics, and dynamics of convergent sand wedges. Journal of Structural Geology 25, 1691–1711.

Marrett, R., Strecker, M.R., 2000. Response of intracontinental deformation in the central Andes to the late Cenozoic reorganization of South American Plate motions. Tectonics 19, 452–467.

Marrett, R.A., Allmendinger, R.W., Alonso, R.N., Drake, R., 1994. Late Cenozoic tectonic evolution of the Puna Plateau and adjacent foreland, northwestern Argentine Andes. Journal of South American Earth Sciences 7, 179–207.

Norabuena, E.O., Dixon, T.H., Stein, S., Harrison, C.G.A., 1999. Decelerating Nazca-South America and Nazca-Pacific plate motions. Geophysical Research Letters 26, 3,405–3,408.

Oncken, O., Sobolev, S., Stiller, M., Asch, G., Haberland, C., Mechie, J., Yuan, X.H., Lüschen, E., Giese, P., Wigger, P., Lüth, S., Scheuber, E., Götze, H.J., Brasse, H., Buske, S., Yoon, M.K., Shapiro, S., Rietbrock, A., Chong, G., Wilke, H.G., González, G., Bravo, P., Vieytes, H., Martinez, E., Rössling, R., Ricaldi, E., 2003. Seismic imaging of a convergent continental margin and plateau in the central Andes (Andean Continental Research Project 1996 (ANCORP' 96)). Journal of Geophysical Research 108, 2328. doi:10.1029/2002JB001771.

Oncken, O., Hindle, D., Kley, J., Elger, K., Victor, P., Schemmann, K., 2006. Deformation of the Central Andean upper plate system – facts, fiction, and constraints for plateau models. In: Oncken, O., Chong, G., Franz, G., Giese, P., Götze, H.-J., Ramos, V., Strecker, M., Wigger, P. (Eds.), The Andes – Active Subduction Orogeny. Springer, pp. 3–27.

Pardo-Casas, F., Molnar, P., 1987. Relative motion of Nazca (Farallon) and South American plates since Late Cretaceous time. Tectonics 6, 233–248.

Park, R.G., 1981. Shear zone deformation and bulk strain in granite–greenstone terrain of the Western Superior Province. Precambrian Research 14, 31–47.

Petrinovic, I.A., Riller, U., Brod, J.A., 2005. The Negra Muerta Volcanic Complex, southern central Andes: geochemical characteristics and magmatic evolution of an episodically active volcanic centre. Journal of Volcanology and Geothermal Research 140, 295–320.

Petrinovic, I.A., Riller, U., Alvarado, G., Brod, J.A., Arnosio, M., 2006. Bimodal volcanism in a tectonic transfer zone: evidence for tectonically controlled magmatism in the southern Central Andes, NW Argentina. Journal of Volcanology and Geothermal Research 152, 240–252.

Quimet, W.B., Cook, K.L., 2010. Building the central Andes through axial lower crustal flow. Tectonics 29, TC3010. doi:10.1029/2009TC002460.

Ramelow, J., Riller, U., Romer, R.L., Oncken, O., 2006. Kinematic link between episodic caldera collapse of the Negra Muerta Collapse Caldera and motion on the Olacapato–El Toro Fault Zone, NW-Argentina. International Journal of Earth Sciences 95, 529–541. doi:10.1007/s00531-005-0042-x.

Riller, U., Oncken, O., 2003. Growth of the central Andean Plateau by tectonic segmentation is controlled by the gradient in crustal shortening. Journal of Geology 111, 367–384.

Riller, U., Petrinovic, I., Ramelow, J., Strecker, M., Oncken, O., 2001. Late Cenozoic tectonism, caldera and plateau formation in the central Andes. Earth and Planetary Science Letters 188, 299–311.

Schellart, W., 2000. Shear test results for cohesion and friction coefficients for different granular materials: scaling implications for their usage in analogue modelling. Tectonophysics 324, 1–16.

Scheuber, E., Andriessen, P.A.M., 1990. The kinematic significance of the Atacama Fault Zone, northern Chile. Journal of Structural Geology 12, 243–257.

Schmitz, M., Heinsohn, W.-D., Schilling, F.R., 1997. Seismic, gravity, and petrological evidence for the partial melt beneath the thickened Central Andean crust (21–23°). Tectonophysics 270, 313–326.

Schueller, S., Davy, P., 2008. Gravity influenced brittle–ductile deformation and growth faulting in the lithosphere during collision: Results from laboratory experiments. Journal of Geophysical Research 113 (B12). doi:10.1029/2007JB005560.

Schueller, S., Gueydan, F., Davy, P., 2010. Mechanics of the transition from localized to distributed fracturing in layered brittle–ductile systems. Tectonophysics 484, 48–59. doi:10.1016/j.tecto.2009.09.008.

Sobel, E.R., Hilley, G.E., Strecker, M.R., 2003. Formation of internally-drained contractional basins by aridity-limited bedrock incision. Journal of Geophysical Research 108, 2344. doi:10.1029/2002JB001883.

Trumbull, R.B., Riller, U., Oncken, O., Scheuber, E., Munier, K., Hongn, F., 2006. The time–space distribution of Cenozoic volcanism in the south-central Andes: a new data compilation and some tectonic implications. In: Oncken, O., Chong, G., Franz, G., Giese, P., Götze, H.-J., Ramos, V.A., Strecker, M.R., Wigger, P. (Eds.), The Andes – Active Subduction Orogeny. Springer, pp. 29–43.

Urreiztieta, M., Gapais, D., Le Corre, C., Cobbold, P.R., Rossello, E., 1996. Cenozoic dextral transpression and basin development at the southern edge of the Puna plateau, northwestern Argentina. Tectonophysics 254, 17–39.

Weijermars, R., 1986. Flow behaviour and physical chemistry of bouncing putties and related polymers in view of tectonic laboratory. Tectonophysics 124, 325–358.

Yuan, X., Sobolev, S.V., Kind, R., Oncken, O., Bock, G., Asch, G., Schurr, B., Graeber, F., Rudloff, A., Hanka, W., Wylegalla, K., Tibi, R., Haberland, Ch., Rietbrock, A., Giese, P., Wigger, P., Röwer, P., Zandt, G., Beck, S., Wallace, T., Pardo, M., Comte, D., 2000. Subduction and collision processes in the Central Andes constrained by converted seismic phases. Nature 408, 958–961.